Adaptive Filtering for Multi-Sensor Maneuvering Cislunar Space Object Tracking

John L. Iannamorelli
Purdue University
Keith A. LeGrand
Purdue University

ABSTRACT

Successful space domain awareness (SDA) requires maintaining track custody of cooperative and noncooperative cislunar space objects (CSOs) through both ballistic and maneuvering trajectories. The surveillance of CSOs is particularly challenging due to the underlying chaotic multi-body dynamics, which makes future motion harder to predict compared to Keplerian orbits. While methods exist for tracking cooperative spacecraft using high accuracy range measurements, the problem of passive noncooperative maneuvering CSO tracking has received considerably less attention. In this paper, CSO motion is modeled as a jump Markov system (JMS), where the CSO modality is unknown and subject to random switching. A novel adaptive Bayesian filter is proposed and shown to successfully maintain CSO track custody through both ballistic and maneuvering phases of an Artemis I-like trajectory.

1. INTRODUCTION

Accurate knowledge of a space object's orbit and its associated uncertainty is essential to cislunar space domain awareness (SDA). The probabilistic approach to cislunar space object (CSO) tracking involves finding complete statistical descriptions of state uncertainty conditioned on available noisy observations. Uncertainty realism in cislunar SDA is critical not only for state estimation accuracy, but for downstream objectives including conjunction analysis [1], object search [2], and multi-sensor fusion [3]. Tracking a CSO with sparse observations presents significant estimation challenges due in part to the underlying nonlinear, chaotic multi-body dynamics, which result in highly non-Gaussian state distributions. Notional cislunar space-based observer constellations [4] increase observation opportunities yet are still limited by Moon occlusion and albedo, which prevent consistent measurement opportunities, specifically during close approaches to the Moon. During observation gaps, CSO state uncertainty grows rapidly and exhibits a highly non-Gaussian structure driven by the underlying nonlinear and chaotic multi-body dynamics, even when the CSO is assumed to be ballistic. Tracking a maneuvering CSO is even more challenging, as the unknown time and magnitude of CSO maneuvers accelerate uncertainty growth.

In the Bayesian approach to state estimation and tracking, full statistical descriptions of the target uncertainty are sought, typically in the form of probability density functions (pdfs). In nonlinear settings, Bayesian Gaussian mixture (GM) and particle filters offer distinct advantages in that their underlying parameterizations can accurately approximate arbitrary non-Gaussian pdfs, as illustrated in Fig. 1(a). Adaptive Gaussian mixture (AGM) filter approaches [5–10] systematically increase and decrease the mixture resolution in key regions of the distribution support to account for strong nonlinear effects while maintaining overall efficiency. Applications of AGM filtering to near-Earth and CSO tracking are demonstrated in [7, 11] and [12], respectively. Other notable nonlinear estimation approaches include, for example, polynomial chaos expansion [13, 14], conjugate unscented transform [1], and multi-fidelity methods [15].

The challenging problem of maneuvering target tracking is an extensively studied problem with applications in autonomous vehicle tracking [16, 17], air traffic control [18, 19], and missile defense [20, 21]. Maneuvering objects are commonly modeled as jump Markov systems (JMSs), wherein an object's modality evolves according to a homogeneous Markov chain [22–28]. Each modality consists of its own dynamics and measurement model, and thus can capture different object behaviors, such as ballistic flight and thrusting. The Bayes-optimal filter solution requires exponential complexity to account for the possible target mode histories, motivating suboptimal approximations such as the widely adopted interacting multiple model (IMM) filter [23]. Non-JMS formulations include a control-theoretic approach that detects maneuvers based on the integrated control effort required to connect two boundary states under an assumed

optimal control policy [29–33]. While maneuvering target tracking and Bayesian nonlinear estimation have received extensive attention independently, comparatively little existing work has been dedicated to probabilistic nonlinear estimation of maneuvering objects in chaotic systems.

This paper presents the adaptive Gaussian mixture interacting multiple model (AGMIMM) filter, a novel AGM filter for tracking noncooperative maneuvering objects in chaotic dynamic systems. The AGMIMM filter features a multi-pronged adaptation approach. Unlike existing nonlinear AGM estimators, the AGMIMM adaptively accounts for stochastic target modality changes and, unlike existing maneuvering target trackers, employs a comprehensive multi-criterion mixture adaptation for other important nonlinear effects. In particular, this paper considers adaptation criteria designed for capturing nonlinear effects from dynamics, measurements, negative information, and known constraints. Another novel contribution of this paper is the adoption of a cluster-based merging algorithm to accurately approximate the entire target mode history, which is shown to significantly improve state estimation performance and robustness compared to existing techniques. The application to multi-sensor noncooperative CSO tracking is then considered, where the maneuvering CSO modality is unknown and subject to random switching. The effectiveness of the new filter is demonstrated in a challenging angles-only tracking problem, where a noncooperative CSO performs multiple unknown maneuvers to achieve an Artemis I-like trajectory. Synthetic angle measurements are generated based on a notional network of cislunar space-based observers flying in a 1:1 resonant orbit configuration.

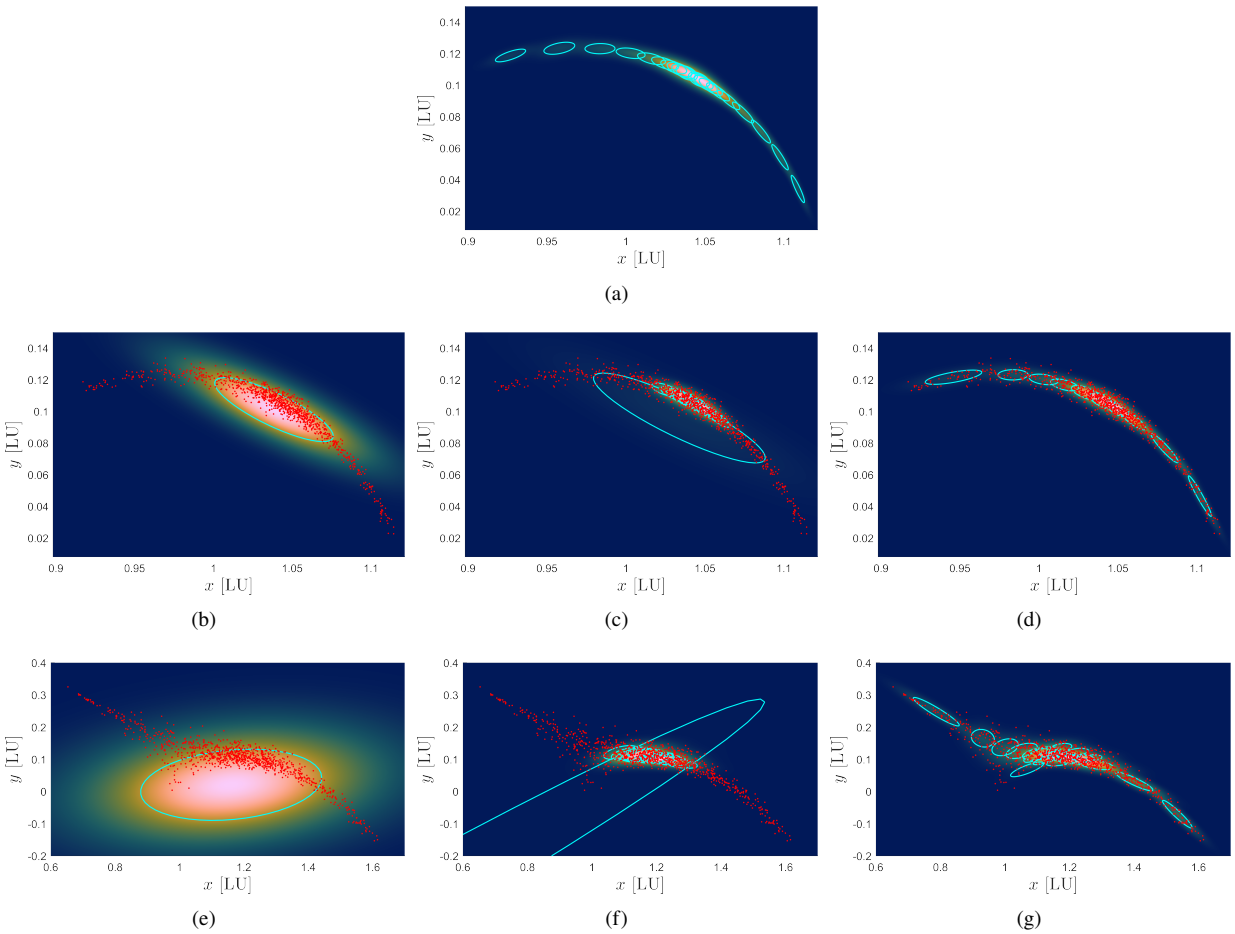

Fig. 1: Comparison of merging and prediction methods where cyan lines denote the 1σ contours of each component and red dots denote 100 Monte Carlo samples of a 20-component GM representing the true mixed mode-conditioned posterior (a). The true distribution is merged using the techniques of the (b) IMM [23], (c) GMIMM [24], and (d) AGMIMM. The merged GMs of the GMIMM and AGMIMM cases have 10 components each. The mixed mode-conditioned posteriors are propagated over five days for the (e) IMM, (f) GMIMM, and (g) AGMIMM.

2. PROBLEM FORMULATION

This paper considers the problem of estimating the state and modality of a nocooperative CSO conditioned on all available sensor measurements. Particularly, the CSO state $\mathbf{x}_k \in \mathbb{R}^6$ is defined as

$$\mathbf{x}_k = \begin{bmatrix}\mathbf{r}_k^\top & \mathbf{v}_k^\top\end{bmatrix}^\top = \begin{bmatrix}x_k & y_k & z_k & \dot{x}_k & \dot{y}_k & \dot{z}_k\end{bmatrix}^\top \tag{1}$$

where $(\cdot)_k$ describes the quantities at discrete time t_k, $\mathbf{r}_k \in \mathbb{R}^3$ is the relative position of the target with respect to the Earth-Moon barycenter in the synodic frame, and $\mathbf{v}_k \in \mathbb{R}^3$ is the relative velocity of the target in the synodic frame. Without loss of generality, this paper adopts the circular restricted three-body problem (CR3BP) assumptions. Let μ be the ratio of the mass of the Moon to the sum of the masses of the Moon and Earth, and let $r_{/\mathrm{Earth}}$ and $r_{/\mathrm{Moon}}$ be the distances of the target from the Earth and Moon, respectively. Then, the dynamics of the target are described by the continuous time differential equations

$$\ddot{x} - 2\dot{y} = w_x(t,\tau) + \left.\frac{\partial U}{\partial x}\right|_{\mathbf{x}}, \qquad \ddot{y} + 2\dot{x} = w_y(t,\tau) + \left.\frac{\partial U}{\partial y}\right|_{\mathbf{x}}, \qquad \ddot{z} = w_z(t,\tau) + \left.\frac{\partial U}{\partial z}\right|_{\mathbf{x}} \tag{2}$$

$$U = \frac{1-\mu}{r_{/\mathrm{Earth}}} + \frac{\mu}{r_{/\mathrm{Moon}}} + \frac{x^2+y^2}{2} \tag{3}$$

where U is the pseudo-potential and $\mathbf{w}(t,\tau) = \begin{bmatrix}w_x(t,\tau) & w_y(t,\tau) & w_z(t,\tau)\end{bmatrix}^\top$ is the mode-dependent relative acceleration due to unknown inputs such as target thrust. If $\mathbf{w}(t,\tau) = \mathbf{0}$, then CR3BP equations of motion (EOMs) admit an integral of motion known as the Jacobi constant and defined as

$$C(\mathbf{x}_k) = 2U - \mathbf{v}_k^\top \mathbf{v}_k \tag{4}$$

This paper assumes that target mode changes (e.g., from ballistic to thrusting) occur at discrete time steps and thus form a sequence $(\tau_0, \tau_1, \ldots, \tau_k)$. Because the modes are unknown a priori, they are modeled as a homogeneous Markov chain with known mode transition probabilities

$$\pi_{ij} = \Pr(\tau_k = j | \tau_{k-1} = i) \tag{5}$$

that are time-invariant and independent of the base state. System modes can take values from the set $\mathcal{M} = \{1, \ldots, M\} \subset \mathbb{N}$ where M is the number of possible modes. The target mode τ_k is defined to be left-continuous such that mode τ_k is in effect over $t \in [t_{k-1}^+, t_k^-]$.

Angles-only measurements of the target are taken by a network of O space-based observers each endowed with a body frame

$$\mathcal{B}^{(o)} = (\mathbf{r}_{\mathrm{obs}}^{(o)}, \hat{\mathbf{b}}_1^{(o)}, \hat{\mathbf{b}}_2^{(o)}, \hat{\mathbf{b}}_3^{(o)}) \tag{6}$$

where $\mathbf{r}_{\mathrm{obs}}^{(o)}$ is the position of observer o with respect to the Earth-Moon barycenter in the synodic frame and $\hat{\mathbf{b}}_1^{(o)}$, $\hat{\mathbf{b}}_2^{(o)}$, and $\hat{\mathbf{b}}_3^{(o)}$ are unit vectors that form an orthogonal basis. Each observer is equipped with a camera whose boresight coincides with the $\hat{\mathbf{b}}_2^{(o)}$ direction. The transformations from the synodic frame to each observer body frame are assumed known. The observer state $\boldsymbol{\xi}^{(o)}$ consists of observer o's relative position and orientation and determines the bounded sensor field-of-view (FoV) $\mathcal{S}^{(o)}(\boldsymbol{\xi}^{(o)})$, where $\mathcal{S}^{(o)}$ is taken to be a compact and bounded set in $\mathbb{R}^3$. Observer o is capable of measuring the target if and only if the target is within $\mathcal{S}^{(o)}$, illuminated, not occluded by the Earth/Moon, and not in the Moon exclusion angle (see Fig. 2). Then, the probability of detection for each observer is defined as

$$p_{D,k}^{(o)}(\mathbf{x}; \mathcal{S}^{(o)}) = 1_{\mathcal{S}^{(o)}}(\mathbf{r}) \times \psi(\mathbf{x}, \boldsymbol{\xi}^{(o)}) \tag{7}$$

where the indicator function

$$1_B(\mathbf{a}) \triangleq \begin{cases} 1 & \mathbf{a} \in B \\ 0 & \text{otherwise} \end{cases} \tag{8}$$

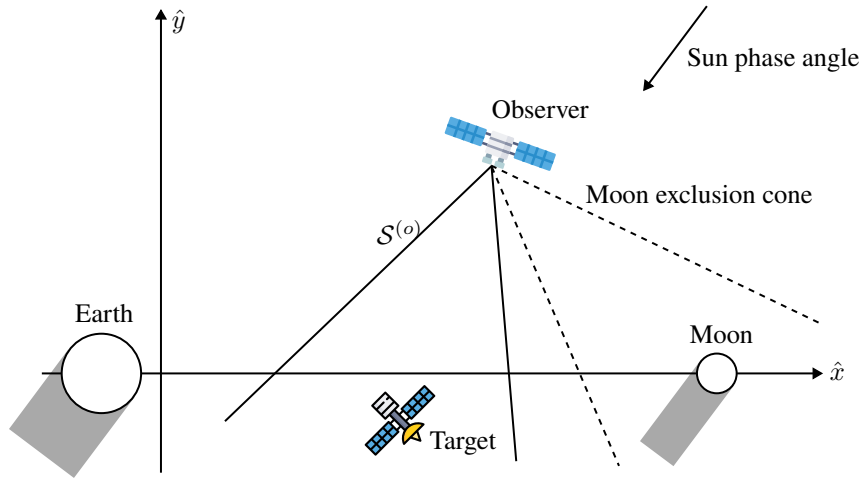

Fig. 2: Example configuration where the target is within the bounded sensor FoV, illuminated, not occluded by the Earth/Moon, and not in the Moon exclusion angle (note: Earth, Moon, target, and observer are not to scale).

and $\psi(\mathbf{x}, \boldsymbol{\xi}^{(o)})$ is unity if the target is illuminated, non-occluded, and outside of the Moon exclusion angle for observer o and zero otherwise.

The angles-only measurements come in the form of azimuth θ and elevation ϕ angles. For each observer, these measurements are concatenated into the measurement vector $\mathbf{z}^{(o)} = \begin{bmatrix}\theta^{(o)} & \phi^{(o)}\end{bmatrix}^\top$ defined by the nonlinear map

$$\mathbf{z}^{(o)} = \mathbf{h}^{(o)}(\mathbf{x}, \tau) = \begin{bmatrix} \arctan\left(\frac{\hat{\mathbf{u}}^{(o)} \cdot \hat{\mathbf{b}}_1^{(o)}}{\hat{\mathbf{u}}^{(o)} \cdot \hat{\mathbf{b}}_2^{(o)}}\right) \\ \arcsin\left(\hat{\mathbf{u}}^{(o)} \cdot \hat{\mathbf{b}}_3^{(o)}\right) \end{bmatrix} \tag{9}$$

where

$$\hat{\mathbf{u}}^{(o)} = \frac{\mathbf{r} - \mathbf{r}_{\text{obs}}^{(o)}}{\|\mathbf{r} - \mathbf{r}_{\text{obs}}^{(o)}\|} \tag{10}$$

At each observation time k, observer o produces a Bernoulli random finite set (RFS) measurement $Z_k^{(o)}$ that is either empty or contains a single vector measurement $\mathbf{z}_k^{(o)}$, depending on the probability of detection. The multi-sensor measurement Z_k is then defined as the tuple

$$Z_k \triangleq (Z_k^{(1)}, \ldots, Z_k^{(O)}) \tag{11}$$

This paper assumes that the continuous-time dynamics can be accurately approximated as a discrete-time nonlinear JMS

$$\mathbf{x}_k = \mathbf{f}(\mathbf{x}_{k-1}, \tau_k) + \mathbf{w}_{k-1}(\tau_k) \tag{12}$$

$$\mathbf{z}_k^{(o)} = \mathbf{h}^{(o)}(\mathbf{x}_k, \tau_k) + \boldsymbol{\nu}_k(\tau_k) \tag{13}$$

where $\mathbf{f}(\mathbf{x}, \tau)$ is defined as the solution to the CR3BP EOMs and the process noise $\mathbf{w}_{k-1}(\tau_k)$ and measurement noise $\boldsymbol{\nu}_k(\tau_k)$ are zero-mean, Gaussian, and white with covariances $\mathrm{E}[\mathbf{w}_{k-1}(\tau_k)\mathbf{w}_{k-1}(\tau_k)^\top] = \mathbf{Q}_{k-1}(\tau_k)$ and $\mathrm{E}[\boldsymbol{\nu}_k(\tau_k)\boldsymbol{\nu}_k(\tau_k)^\top] = \mathbf{R}_k(\tau_k)$. The target kinematic state (also known as the base state) and modality are correlated and thus modeled as the joint state $\tilde{\mathbf{x}}_k = \begin{bmatrix}\mathbf{x}_k^\top & \tau_k\end{bmatrix}^\top$. With assumed knowledge of the pdf $p_0(\tilde{\mathbf{x}}_0)$ at some time t_0, this paper considers the problem of recursively estimating the unknown prior and posterior conditional distributions, $p_{k|k-1}(\tilde{\mathbf{x}}_k|Z_{0:k-1})$ and $p_k(\tilde{\mathbf{x}}_k|Z_{0:k})$, respectively, where $Z_{0:k}$ denotes the entire measurement history from t_0 to t_k. The evolution of these densities follows

$$\ldots \to p_{k-1}(\tilde{\mathbf{x}}_{k-1}|Z_{0:k-1}) \to p_{k|k-1}(\tilde{\mathbf{x}}_k|Z_{0:k-1}) \to p_k(\tilde{\mathbf{x}}_k|Z_{0:k}) \to \ldots \tag{14}$$

3. METHODOLOGY

This paper presents a novel adaptive Bayesian filter that is designed to handle the challenging angles-only tracking problem of a maneuvering target in cislunar space in the presence of long observation gaps. Such a problem experiences strong nonlinearities in both the dynamics and measurement functions. The nonlinearities combined with the chaotic nature of the CR3BP results in highly non-Gaussian distributions that prevent the adoption of typical central moment filters which is even more evident with the introduction of maneuvers with unknown time and magnitude. This paper presents the AGMIMM where pdfs are represented by GMs with automatic component splitting to account for chaotic dynamics, nonlinear measurements, bounded sensor FoVs, and other nonlinear constraints. The AGMIMM utilizes the foundation of the IMM that allows for approximations of a nonlinear JMS filter to reduce computational cost [23].

3.1 Nonlinear JMS Bayes Filter

In a system modeled as a nonlinear JMS, both the target's state and modality are estimated. Let $g_k(Z_k|\tilde{\mathbf{x}})$ denote the joint multi-sensor likelihood function. Given the multi-sensor measurement Z_k and prior $p_{k|k-1}(\tilde{\mathbf{x}})$, the posterior distribution is given by Bayes' rule as

$$p_{k|k}(\tilde{\mathbf{x}}|Z_{0:k}) = \frac{g_k(Z_k|\tilde{\mathbf{x}})p_{k|k-1}(\tilde{\mathbf{x}})}{\int \sum_{\ell=1}^{M} g_k(Z_k|\tilde{\mathbf{x}}^{(\ell)})p(\tilde{\mathbf{x}}^{(\ell)})d\mathbf{x}} \tag{15}$$

where the notation $\tilde{\mathbf{x}}^{(j)} = \begin{bmatrix}\mathbf{x}_k^\top & \tau_k = j\end{bmatrix}^\top$ exposes the modality value. Assuming that measurements are conditionally independent of the target kinematic state and mode, the joint multi-sensor measurement likelihood is given by the product

$$g_k(Z_k|\tilde{\mathbf{x}}) = \prod_{o=1}^{O} g_k^{(o)}(Z_k^{(o)}|\tilde{\mathbf{x}}) \tag{16}$$

By this factorization, the multi-sensor Bayes' update can be written as the composition of single-sensor updates as

$$p_k(\tilde{\mathbf{x}}_k^{(j)}|Z_{0:k}) = \Psi_k^{(O)} \circ \cdots \circ \Psi_k^{(1)} p_{k|k-1}(\tilde{\mathbf{x}}_k^{(j)}|Z_{0:k-1}) \tag{17}$$

as shown in [34], where the single-sensor Bayes update operator $\Psi_k^{(o)}$ is

$$[\Psi_k^{(o)} p](\tilde{\mathbf{x}}) = \frac{g_k^{(o)}(Z_k^{(o)}|\tilde{\mathbf{x}})p(\tilde{\mathbf{x}})}{\int \sum_{\ell=1}^{M} g_k^{(o)}(Z_k^{(o)}|\tilde{\mathbf{x}}^{(\ell)})p(\tilde{\mathbf{x}}^{(\ell)})d\mathbf{x}} \tag{18}$$

and $g_k^{(o)}(Z_k^{(o)}|\tilde{\mathbf{x}}_k^{(j)})$ is the measurement likelihood function for observer o.

The filter prediction step is a direct result of the Chapman-Kolmogorov equation and total probability theorem and is given by

$$p_{k|k-1}(\tilde{\mathbf{x}}_k^{(j)}|Z_{0:k-1}) = \int \sum_{i=1}^{M} p_{k|k-1}(\tilde{\mathbf{x}}_k^{(j)}|\tilde{\mathbf{x}}_{k-1}^{(i)}) p_{k-1}(\tilde{\mathbf{x}}_{k-1}^{(i)}|Z_{0:k-1}) d\mathbf{x}_{k-1} \tag{19}$$

where the joint state transition density $p_{k|k-1}(\tilde{\mathbf{x}}_k^{(j)}|\tilde{\mathbf{x}}_{k-1}^{(i)})$ is known and specified by the mode transition probabilities, dynamics function, and process noise model. Closed-form solutions of (17) and (19) are available when $p_0(\mathbf{x}_0)$ is Gaussian and the state transition and measurement likelihood are linear-Gaussian, yet require $\mathcal{O}(M^k)$ terms. Together, the Markov chain-driven exponential complexity, nonlinear dynamics, and nonlinear observations considered in this paper necessitate suboptimal approximations for tractability.

The joint distribution is readily factored into the mode-conditioned densities and mode probabilities. The prior and posterior pdfs of $\mathbf{x}_k$ conditioned on the jth system mode are defined as

$$p_{k|k-1}^{(j)}(\mathbf{x}_k) = p_{k|k-1}(\mathbf{x}_k|\tau_k = j, Z_{0:k-1}) \tag{20}$$

$$p_k^{(j)}(\mathbf{x}_k) = p_k(\mathbf{x}_k|\tau_k = j, Z_{0:k}) \tag{21}$$

where the superscripts denote the assumed system mode. Let $\mu_{k-1}^{(i)}$ denote the posterior probability of mode i at time t_{k-1} defined as

$$\mu_{k-1}^{(i)} = \Pr(\tau_{k-1} = i | Z_{0:k-1}) \tag{22}$$

and $\bar{\mu}_{k|k-1}^{(j)}$ denote the prior probability of mode j at time t_k defined as

$$\bar{\mu}_{k|k-1}^{(j)} = \Pr(\tau_k = j | Z_{0:k-1}) = \sum_{i=1}^{M} \pi_{ij} \mu_{k-1}^{(i)} \tag{23}$$

The single sensor update operator applied to an arbitrary mode-conditioned density $p^{(j)}(\mathbf{x})$ and prior mode probability $\bar{\mu}^{(j)}$ is defined as

$$[\Psi_k^{(o,j)} p^{(j)}](\mathbf{x}) = \frac{g_k^{(o,j)}(Z_k^{(o)}|\mathbf{x}) p^{(j)}(\mathbf{x})}{\int \sum_{\ell=1}^{M} g_k^{(o,\ell)}(Z_k^{(o)}|\mathbf{x}) p^{(\ell)}(\mathbf{x}) d\mathbf{x}} \tag{24}$$

$$[\Psi_k^{(o,j)} \bar{\mu}^{(j)}] = \frac{p_k^{(o,j)}(Z_k^{(o)}|Z_{0:k-1}) \bar{\mu}^{(j)}}{\sum_{\ell=1}^{M} p_k^{(o,\ell)}(Z_k^{(o)}|Z_{0:k-1}) \bar{\mu}^{(\ell)}} \tag{25}$$

where

$$g_k^{(o,j)}(Z_k^{(o)}|\mathbf{x}) = g_k^{(o)}(Z_k^{(o)}|\tau_k = j, \mathbf{x}) \tag{26}$$

$$p_k^{(o,j)}(Z_k^{(o)}|Z_{0:k-1}) = p_k^{(o)}(Z_k^{(o)}|\tau_k = j, Z_{0:k-1}) \tag{27}$$

Then, the mode-conditioned multi-sensor Bayes' filter equations follow from (19) and (17) and are given by

$$p_{k|k-1}^{(j)}(\mathbf{x}_k) = \int p_{k|k-1}(\mathbf{x}_k|\mathbf{x}_{k-1}, \tau_k = j) p_{k-1}(\mathbf{x}_{k-1}|\tau_k = j, Z_{0:k-1}) d\mathbf{x}_{k-1} \tag{28}$$

$$p_k^{(j)}(\mathbf{x}_k) = \Psi_k^{(O,j)} \circ \cdots \circ \Psi_k^{(1,j)} p_{k|k-1}^{(j)}(\mathbf{x}_k|Z_{0:k-1}) \tag{29}$$

where $p_{k-1}(\mathbf{x}_{k-1}|\tau_k = j, Z_{0:k-1})$ is referred to as the mixed mode-conditioned posterior pdf and is given as

$$p_{k-1}(\mathbf{x}_{k-1}|\tau_k = j, Z_{0:k-1}) = \sum_{i=1}^{M} \left[\frac{\pi_{ij} \mu_{k-1}^{(i)}}{\bar{\mu}_{k|k-1}^{(j)}} p_{k-1}^{(i)}(\mathbf{x}_{k-1}) \right] \tag{30}$$

The update of the prior mode probability $\bar{\mu}_{k|k-1}^{(j)}$ is defined as

$$\mu_k^{(j)} = \Psi_k^{(O,j)} \circ \cdots \circ \Psi_k^{(1,j)} \bar{\mu}_{k|k-1}^{(j)} \tag{31}$$

The remainder of this section is organized as follows: Section 3.2 presents a novel application of a cluster-based merging algorithm to approximate (30) in order to maintain reasonable computational complexity, Section 3.3 discusses the approximations of (28) and (29), and Section 3.4 defines the criteria that informs the adaptive splitting techniques.

3.2 Bayesian IMM Approximations

In the application of the recursion defined in (28) and (29), calculation of the mixed mode-conditioned posterior results in a pdf with an exponentially growing number of terms. Assuming that the posterior pdf $p_{k-1}^{(i)}(\mathbf{x}_{k-1})$ is modeled as the GM

$$p_{k-1}^{(i)}(\mathbf{x}_{k-1}) = \sum_{\ell=1}^{L_{k-1}^{(i)}} \omega_{k-1}^{(\ell,i)} \mathcal{N}(\mathbf{x}_{k-1}; \mathbf{m}_{k-1}^{(\ell,i)}, \mathbf{P}_{k-1}^{(\ell,i)}) \tag{32}$$

where the superscript $(\cdot)^{(\ell,i)}$ denotes the ℓth component for the assumed mode $\tau_{k-1} = i$. The resulting mixed mode-conditioned posterior is then a $\left(\sum_{i=1}^{M} L_{k-1}^{(i)}\right)$-component GM

$$p_{k-1}(\mathbf{x}_{k-1}|\tau_k = j, Z_{0:k-1}) = \sum_{i=1}^{M} \sum_{\ell=1}^{L_{k-1}^{(i)}} \frac{\pi_{ij}\mu_{k-1}^{(i)}}{\bar{\mu}_{k|k-1}^{(j)}} \omega_{k-1}^{(\ell,i)} \mathcal{N}(\mathbf{x}_{k-1}; \mathbf{m}_{k-1}^{(\ell,i)}, \mathbf{P}_{k-1}^{(\ell,i)}) \tag{33}$$

In successive time steps, the number of components of the mixed mode-conditioned posterior grows exponentially necessitating the need for suboptimal approximations to retain computational tractability. At each time step, the mixed mode-conditioned posterior is approximated as

$$p_{k-1}(\mathbf{x}_{k-1}|\tau_k = j, Z_{0:k-1}) \approx \sum_{\ell=1}^{L} \omega_{k-1|k-1}^{(\ell,j)} \mathcal{N}(\mathbf{x}_{k-1|k-1}; \mathbf{m}_{k-1|k-1}^{(\ell,j)}, \mathbf{P}_{k-1|k-1}^{(\ell,j)}) \tag{34}$$

where $L < \sum_{i=1}^{M} L_{k-1}^{(i)}$ and the subscript $(\cdot)_{k-1|k-1}$ and superscript $(\cdot)^{(\ell,j)}$ delineate the approximate weights and pdfs in (34) from those seen in (33).

The most notable approximation is the IMM, where $L = 1$ and the mode-conditioned pdfs are assumed Gaussian [23]. As such, the mixed mode-conditioned posterior is approximated as

$$p_{k-1}(\mathbf{x}_{k-1}|\tau_k = j, Z_{0:k-1}) \approx \mathcal{N}(\mathbf{x}_{k-1}; \mathbf{m}_{k-1|k-1}^{(j)}, \mathbf{P}_{k-1|k-1}^{(j)}) \tag{35}$$

where the mean $\mathbf{m}_{k-1|k-1}^{(j)}$ and covariance $\mathbf{P}_{k-1|k-1}^{(j)}$ are chosen to match the moments of (33). The assumption of Gaussianity is reasonable in some cases but not where highly nonlinear and chaotic dynamics result in highly non-Gaussian distributions (as evidenced by numerical experiments conducted in [35]).

The GMIMM generalizes the IMM to account for GM representations of the mode-conditioned pdfs [24]. The mixed mode-conditioned posterior is approximated by retaining the r components with the highest weights and merging the remaining components into a single Gaussian using moment-matching techniques. In other words, $L = r + 1$ and the mixed mode-conditioned posterior is approximated as

$$p_{k-1}(\mathbf{x}_{k-1}|\tau_k = j, Z_{0:k-1}) \approx \sum_{\ell=1}^{r+1} \omega_{k-1|k-1}^{(\ell,j)} \mathcal{N}(\mathbf{x}_{k-1}; \mathbf{m}_{k-1|k-1}^{(\ell,j)}, \mathbf{P}_{k-1|k-1}^{(\ell,j)}) \tag{36}$$

As evidenced by Figs. 1(b) and 1(c), both the approximation methods of the IMM and GMIMM fail to accurately model the true mixed mode-conditioned posterior. In both cases, the approximations underestimate the distribution tails while introducing erroneous probability mass in low-probability regions of the support.

This paper proposes a new approximation of the mixed mode-conditioned posterior based on recent advances in GM reduction methods. Specifically, the AGMIMM filter incorporates the cluster-based merging algorithm of [36] to efficiently approximate the mixed mode-conditioned posterior while minimizing the integrated square distance between the true and approximate density. The Gaussian mixture reduction via clustering (GMRC) merging algorithm takes a two-pronged approach, where a greedy reduction algorithm is applied to obtain an initial guess and the k-means algorithm is applied to the original GM to provide an accurate reduction of components. The proposed filter uses Runnals' merging algorithm as the GMRC's initial guess [37]. The mixed mode-conditioned posterior is then approximated as

$$p_{k-1}(\mathbf{x}_{k-1}|\tau_k = j, Z_{0:k-1}) \approx \sum_{\ell=1}^{L} \omega_{k-1|k-1}^{(\ell,j)} \mathcal{N}(\mathbf{x}_{k-1}; \mathbf{m}_{k-1|k-1}^{(\ell,j)}, \mathbf{P}_{k-1|k-1}^{(\ell,j)}) \tag{37}$$

where $L < \sum_{i=1}^{M} L_{k-1}^{(i)}$ is the desired number of components and the weights, means, and covariances are found via the GMRC algorithm. Fig. 1(d) presents the approximated mixed mode-conditioned posterior as a good approximation of the original pdf.

3.3 Gaussian Mixture Filter with State-Dependent Detection

With an adequate approximation of the mixed mode-conditioned posterior, by (28), the mode-conditioned prior at t_k is

$$p^{(j)}_{k|k-1}(\mathbf{x}_k) = \sum_{\ell=1}^{L^{(j)}_{k|k-1}} \omega^{(\ell,j)}_{k-1|k-1} \int \mathcal{N}(\mathbf{x}_k; \mathbf{f}^{(j)}(\mathbf{x}_{k-1}), \mathbf{Q}^{(j)}_{k-1}) \mathcal{N}(\mathbf{x}_{k-1}; \mathbf{m}^{(\ell,j)}_{k-1|k-1}, \mathbf{P}^{(\ell,j)}_{k-1|k-1}) d\mathbf{x}_{k-1} \tag{38}$$

A closed-form solution of (38) is not available, in general, for systems with nonlinear dynamics. For sufficiently small covariances, the mode-conditioned prior pdf can be approximated with moment-matching techniques as the GM [38]

$$p^{(j)}_{k|k-1}(\mathbf{x}_k) \approx \sum_{\ell=1}^{L^{(j)}_{k|k-1}} \omega^{(\ell,j)}_{k|k-1} \mathcal{N}(\mathbf{x}_k; \mathbf{m}^{(\ell,j)}_{k|k-1}, \mathbf{P}^{(\ell,j)}_{k|k-1}) \tag{39}$$

where

$$\omega^{(\ell,j)}_{k|k-1} = \omega^{(\ell,j)}_{k-1|k-1} \tag{40}$$

$$\mathbf{m}^{(\ell,j)}_{k|k-1} = \int \mathbf{f}^{(j)}(\mathbf{x}_{k-1}) \mathcal{N}(\mathbf{x}_{k-1}; \mathbf{m}^{(\ell,j)}_{k-1|k-1}, \mathbf{P}^{(\ell,j)}_{k-1|k-1}) d\mathbf{x}_{k-1} \tag{41}$$

$$\mathbf{P}^{(\ell,j)}_{k|k-1} = \int (\mathbf{f}^{(j)}(\mathbf{x}_{k-1}) - \mathbf{m}^{(\ell,j)}_{k|k-1})(\mathbf{f}^{(j)}(\mathbf{x}_{k-1}) - \mathbf{m}^{(\ell,j)}_{k|k-1})^\top \mathcal{N}(\mathbf{x}_{k-1}; \mathbf{m}^{(\ell,j)}_{k-1|k-1}, \mathbf{P}^{(\ell,j)}_{k-1|k-1}) d\mathbf{x}_{k-1} + \mathbf{Q}^{(j)}_{k-1} \tag{42}$$

It is important to consider the validity of the assumption that the covariances are small enough for (39) to be valid. Specifically, the covariances should be small enough so that deviations in $\mathbf{m}^{(\ell,j)}_{k-1|k-1}$ behave linearly over t_{k-1} to t_k. This requirement provides the central idea of adaptive GM filtering discussed in Section 3.4.

Following the prediction step, the mode-conditioned prior is updated iteratively by the single sensor update operator $\Psi^{(o,j)}_k$. Let the mode-conditioned pdf be a GM of the form

$$p^{(j)}(\mathbf{x}) = \sum_{\ell=1}^{L^{(j)}} \omega^{(\ell,j)} \mathcal{N}(\mathbf{x}; \mathbf{m}^{(\ell,j)}, \mathbf{P}^{(\ell,j)}) \tag{43}$$

The single-sensor RFS measurement likelihood is given by

$$g^{(o,j)}_k(Z^{(o)}_k|\mathbf{x}_k) = \begin{cases} 1 - p^{(o)}_{D,k}(\mathbf{x}_k; \mathcal{S}^{(o)}) & Z^{(o)}_k = \emptyset \\ p^{(o)}_{D,k}(\mathbf{x}_k; \mathcal{S}^{(o)}) g^{(o,j)}_k(\mathbf{z}^{(o)}_k|\mathbf{x}_k) & Z^{(o)}_k = \{\mathbf{z}_k\} \end{cases} \tag{44}$$

and accounts for both measurement noise and missed detections. Then, by (18), each single-sensor iteration of the multi-sensor Bayes update yields an updated mode-conditioned pdf of the form

$$\begin{aligned} [\Psi^{(o,j)}_k p^{(j)}](\mathbf{x}) \propto & 1_\emptyset(Z^{(o)}_k) \sum_{\ell=1}^{L^{(j)}} (1 - p_{D,k}(\mathbf{x}; \mathcal{S}^{(o)})) \omega^{(\ell,j)} \mathcal{N}(\mathbf{x}; \mathbf{m}^{(\ell,j)}, \mathbf{P}^{(\ell,j)}) \\ & + (1 - 1_\emptyset(Z^{(o)}_k)) \sum_{\ell=1}^{L^{(j)}} p_{D,k}(\mathbf{x}; \mathcal{S}^{(o)}) \omega^{(\ell,j)} \prod_{\mathbf{z} \in Z^{(o)}_k} g^{(o,j)}_k(\mathbf{z}|\mathbf{x}_k) \mathcal{N}(\mathbf{x}; \mathbf{m}^{(\ell,j)}, \mathbf{P}^{(\ell,j)}) \end{aligned} \tag{45}$$

where the single-sensor measurement likelihood function is $g^{(o,j)}_k(\mathbf{z}|\mathbf{x}_k) = \mathcal{N}(\mathbf{z}; \mathbf{h}^{(o,j)}(\mathbf{x}_k), \mathbf{R}^{(j)}_k)$. Note that, by the RFS-theoretic measurement likelihood and state-dependent probability of detection function, negative information from non-detection is systematically assimilated in a unified Bayes update. On the other hand, the state-dependent probability of detection is nonlinear in $\mathbf{x}$. To that end, a zeroth-order Taylor series expansion can be applied about the means, as shown in [10]. Then, the single sensor update of a mode-conditioned prior is approximated as the GM

$$[\Psi^{(o,j)}_k p^{(j)}](\mathbf{x}) \approx p^{(j)}_+(\mathbf{x}) = \sum_{\ell=1}^{L^{(j)}_+} \omega^{(\ell,j)}_+ \mathcal{N}(\mathbf{x}; \mathbf{m}^{(\ell,j)}_+, \mathbf{P}^{(\ell,j)}_+) \tag{46}$$

where

$$\omega_+^{(\ell,j)} \propto \begin{cases} \omega^{(\ell,j)}(1 - p_{D,k}^{(o)}(\mathbf{m}^{(\ell,j)}; \mathcal{S}^{(o)})) & Z_k^{(o)} = \emptyset \\ \omega^{(\ell,j)} p_{D,k}^{(o)}(\mathbf{m}^{(\ell,j)}; \mathcal{S}^{(o)}) q_+^{(\ell,j)}(\mathbf{z}_k^{(o)}) & Z_k^{(o)} = \{\mathbf{z}_k^{(o)}\} \end{cases} \tag{47}$$

$$\mathbf{m}_+^{(\ell,j)} = \begin{cases} \mathbf{m}^{(\ell,j)} & Z_k^{(o)} = \emptyset \\ \mathbf{m}^{(\ell,j)} + \mathbf{K}_+^{(\ell,j)}(\mathbf{z}_k^{(o)} - \hat{\mathbf{z}}_+^{(\ell,j)}) & Z_k^{(o)} = \{\mathbf{z}_k^{(o)}\} \end{cases} \tag{48}$$

$$\mathbf{P}_+^{(\ell,j)} = \begin{cases} \mathbf{P}^{(\ell,j)} & Z_k^{(o)} = \emptyset \\ \mathbf{P}^{(\ell,j)} - \mathbf{C}_+^{(\ell,j)}(\mathbf{K}_+^{(\ell,j)})^\top - \mathbf{K}_+^{(\ell,j)}(\mathbf{C}_+^{(\ell,j)})^\top + \mathbf{K}_+^{(\ell,j)}\mathbf{P}_{z,+}^{(\ell,j)}(\mathbf{K}_+^{(\ell,j)})^\top & Z_k^{(o)} = \{\mathbf{z}_k^{(o)}\} \end{cases} \tag{49}$$

$$q_+^{(\ell,j)}(\mathbf{z}_k^{(o)}) = \mathcal{N}(\mathbf{z}_k^{(o)}; \hat{\mathbf{z}}_+^{(\ell,j)}, \mathbf{P}_{z,+}^{(\ell,j)}) \tag{50}$$

$$\hat{\mathbf{z}}_+^{(\ell,j)} = \int \mathbf{h}^{(o,j)}(\mathbf{x}) \mathcal{N}(\mathbf{x}; \mathbf{m}^{(\ell,j)}, \mathbf{P}^{(\ell,j)}) d\mathbf{x} \tag{51}$$

$$\mathbf{C}_+^{(\ell,j)} = \int (\mathbf{x} - \mathbf{m}^{(\ell,j)})(\mathbf{h}^{(o,j)}(\mathbf{x}) - \hat{\mathbf{z}}_+^{(\ell,j)})^\top \mathcal{N}(\mathbf{x}; \mathbf{m}^{(\ell,j)}, \mathbf{P}^{(\ell,j)}) d\mathbf{x} \tag{52}$$

$$\mathbf{P}_{z,+}^{(\ell,j)} = \int (\mathbf{h}^{(o,j)}(\mathbf{x}) - \hat{\mathbf{z}}_+^{(\ell,j)})(\mathbf{h}^{(o,j)}(\mathbf{x}) - \hat{\mathbf{z}}_+^{(\ell,j)})^\top \mathcal{N}(\mathbf{x}; \mathbf{m}^{(\ell,j)}, \mathbf{P}^{(\ell,j)}) d\mathbf{x} + \mathbf{R}_k^{(j)} \tag{53}$$

$$\mathbf{K}_+^{(\ell,j)} = \mathbf{C}_+^{(\ell,j)}(\mathbf{P}_{z,+}^{(\ell,j)})^{-1} \tag{54}$$

In addition to the prior mode-conditioned pdf, the prior mode probability $\bar{\mu}_{k|k-1}^{(j)}$ must be updated. Similarly, the single sensor update operator is applied iteratively on $\bar{\mu}_{k|k-1}^{(j)}$ to obtain the posterior mode probability at t_k. Let $\bar{\mu}^{(j)}$ be an arbitrary prior mode probability. Starting from (25) and applying (44), a single iteration of the single sensor update operator is

$$\bar{\mu}_+^{(j)} \propto \begin{cases} \bar{\mu}^{(j)} \sum_\ell^{L_+^{(j)}} \omega^{(\ell,j)}(1 - p_{D,k}^{(o)}(\mathbf{m}^{(\ell,j)}; \mathcal{S}^{(o)})) & Z_k^{(o)} = \emptyset \\ \bar{\mu}^{(j)} \sum_{\ell=1}^{L_+^{(j)}} \omega^{(\ell,j)} p_{D,k}^{(o)}(\mathbf{m}^{(\ell,j)}; \mathcal{S}^{(o)}) q_+^{(\ell,j)}(\mathbf{z}_k^{(o)}) & Z_k^{(o)} = \{\mathbf{z}_k^{(o)}\} \end{cases} \tag{55}$$

under the same zeroth-order Taylor expansion of the detection model about the means.

The single sensor update operator is applied successively on the prior mode probability and the mode-conditioned prior $p_{k|k-1}^{(j)}(\mathbf{x}_k)$ for each observer resulting in the posterior mode probability $\mu_k^{(j)}$ and the mode-conditioned posterior

$$p_k^{(j)}(\mathbf{x}_k) \approx \sum_{\ell=1}^{L_k^{(j)}} \omega_k^{(\ell,j)} \mathcal{N}(\mathbf{x}_k; \mathbf{m}_k^{(\ell,j)}, \mathbf{P}_k^{(\ell,j)}) \tag{56}$$

Closed form solutions of the integrals in (41)-(42) and (51)-(53) are not available when the dynamics and measurement functions are nonlinear, so linearized approximations must be made.

For outputting purposes, the posterior state distribution is found through the total probability theorem and is given by

$$p_k(\mathbf{x}_k | Z_{0:k}) = \sum_{j=1}^{M} \mu_k^{(j)} p_k^{(j)}(\mathbf{x}_k) \tag{57}$$

3.4 Gaussian Mixture Splitting

In problems with nonlinear and chaotic dynamics and nonlinear measurements, the linearized approximations of (41)-(42) and (51)-(53) may only be accurate within small neighborhoods of the component means. Care must then be taken to satisfy the key GM filter assumption that component covariances are commensurately small to ensure linearity within the local support. Adaptive GM filtering addresses these concerns by dynamically increasing the number of components in regions where linear assumptions are most strongly violated. Any component of the GM that violates the assumptions is approximated itself by an R-component GM [5–7].

This paper generalizes splitting as the operator $\tilde{G}_c$ which operates on an arbitrary multivariate GM $p(\mathbf{x})$ as

$$\tilde{G}_c[p(\mathbf{x})] = \sum_{i=1}^{I} G_c[\omega^{(i)}\mathcal{N}(\mathbf{x};\mathbf{m}^{(i)},\mathbf{P}^{(i)})] \tag{58}$$

where

$$G_c[\omega^{(i)}\mathcal{N}(\mathbf{x};\mathbf{m}^{(i)},\mathbf{P}^{(i)})] = \begin{cases} \omega^{(i)}\mathcal{N}(\mathbf{x};\mathbf{m}^{(i)},\mathbf{P}^{(i)}) & c(\omega^{(i)},\mathbf{m}^{(i)},\mathbf{P}^{(i)}) \leq 0 \\ \sum_{\ell=1}^{R} G_c[\omega^{(i,\ell)}\mathcal{N}(\mathbf{x};\mathbf{m}^{(i,\ell)},\mathbf{P}^{(i,\ell)})] & \text{otherwise} \end{cases} \tag{59}$$

and $c(\omega^{(i)},\mathbf{m}^{(i)},\mathbf{P}^{(i)})$ is a splitting criterion. The operator is applied recursively on all newly generated components until no components satisfy the splitting criterion.

Algorithm 1 Single AGMIMM step

Require: Z_k and $\mu_{k-1}^{(i)}$, $p_k^{(i)}(\mathbf{x}_{k-1})\,\forall i \in \mathcal{M}$
  for each $j \in \mathcal{M}$ **do**
    Compute $\bar{\mu}_{k|k-1}^{(j)}$ according to (23)
    Compute $\{\omega_{k-1|k-1}^{(\ell,j)}, \mathbf{m}_{k-1|k-1}^{(\ell,j)}, \mathbf{P}_{k-1|k-1}^{(\ell,j)}\}_{\ell=1}^{L}$ with GMRC algorithm [36]
    Compute $\{\omega_{k|k-1}^{(\ell,j)}, \mathbf{m}_{k|k-1}^{(\ell,j)}, \mathbf{P}_{k|k-1}^{(\ell,j)}\}_{\ell=1}^{L}$ according to (40)-(42)
    $p_{k|k-1}^{(j)}(\mathbf{x}_k) \leftarrow \tilde{G}_c[p_{k|k-1}^{(j)}(\mathbf{x}_k)]$
    $p^{(j)}(\mathbf{x}) \leftarrow p_{k|k-1}^{(j)}(\mathbf{x}_k)$
    $\bar{\mu}^{(j)} \leftarrow \bar{\mu}_{k|k-1}^{(j)}$
    for $o = 1,\ldots,O$ **do**
      $p_+^{(j)}(\mathbf{x}) \leftarrow [\Psi_k^{(o)} p^{(j)}](\mathbf{x})$
      $p^{(j)}(\mathbf{x}) \leftarrow p_+^{(j)}(\mathbf{x})$
      $\bar{\mu}_+^{(j)} \leftarrow [\Psi_k^{(o)} \bar{\mu}^{(j)}]$
      $\bar{\mu}^{(j)} \leftarrow \bar{\mu}_+^{(j)}$
    end for
    $p_k^{(j)}(\mathbf{x}_k) \leftarrow p^{(j)}(\mathbf{x})$
    $\mu_k^{(j)} \leftarrow \bar{\mu}^{(j)}$
    $p_k^{(j)}(\mathbf{x}_k) \leftarrow \tilde{G}_c[p_k^{(j)}(\mathbf{x}_k)]$
  end for
  $p_k(\mathbf{x}_k|Z_{0:k}) \leftarrow \sum_{j=1}^{M} \mu_k^{(j)} p_k^{(j)}(\mathbf{x}_k)$

4. MULTI-SENSOR MANEUVERING CISLUNAR SPACE OBJECT TRACKING

Section 3 presents the framework of the AGMIMM for an arbitrary system with a single iteration outlined in Algorithm 1. The equations are refined in this section to apply the AGMIMM to the problem of maneuvering CSO tracking. Section 4.1 defines a splitting criterion based on statistical linear regression that accounts for errors resulting from the linearization of nonlinear dynamics or measurement functions. Section 4.2 presents a recently proposed splitting criterion for the variance of the Jacobi constant. This criterion aims to combat covariance growth through the CR3BP dynamics as a result of their chaotic nature. Section 4.3 introduces the addition of negative information to utilize non-observations. Section 4.4 adds user-defined constraints on the possible Jacobi constant values and an assumption that the target does not crash into the Moon. Finally, Section 4.5 defines the target modes and develops an approximation of the discrete-time process noise from the assumed continuous-time noise values.

4.1 Statistical Linearization Error Criterion

This paper adopts a statistical linearization approach, where the dynamics and measurement processes are linearized using deterministic weighted sample points. The statistical linear regression approach, which encompasses, for example, unscented, central differencing, and cubature filtering, employs the linear approximation

$$\mathbf{y} = \mathbf{g}(\mathbf{x}) \approx \mathbf{G}\mathbf{x} + \mathbf{b} \tag{60}$$

where the generic nonlinear transformation $\mathbf{g}(\cdot)$ can be replaced by the nonlinear difference equation $\mathbf{f}$ or measurement equation $\mathbf{h}$, and where $\mathbf{G}$ and $\mathbf{b}$ are optimized to minimize the sum of the squares of the linearization error

$$\mathbf{e} = \mathbf{g}(\mathbf{x}) - (\mathbf{G}\mathbf{x} + \mathbf{b}) \tag{61}$$

The statistical linearization approach is particularly attractive for AGM filtering, as the ensemble approximation of the linearization error covariance

$$\mathrm{E}\left[\mathbf{e}\mathbf{e}^\top\right] = \mathbf{P}_e \tag{62}$$

is readily available. With this, the splitting criterion of [39] is adopted, given by

$$c_{\mathrm{SL}}(\omega, \mathbf{m}, \mathbf{P}; \mathbf{g}, s_{\max}, \Gamma) = s - s_{\max} \tag{63}$$

$$s = \omega^\Gamma \cdot (1 - \exp(-\epsilon))^{1-\Gamma} \in [0, 1] \tag{64}$$

$$\epsilon = \mathrm{tr}(\mathbf{P}_e) \tag{65}$$

where Γ and $s_{\max}$ are design parameters and s represents a geometric interpolation of the component weight and linearization error. The tuning parameter $\Gamma \in [0, 1]$ denotes the relative importance of component weight and linearization error in the calculation of the selection criterion; when $\Gamma = 0$, only linearization error is considered, and when $\Gamma = 1$, only component weight is considered [39]. If, for a given component, s exceeds a user-defined threshold $s_{\max}$, the component is split.

4.2 Jacobi Constant Criterion

In addition to the linearization error splitting, the proposed filter employs a newly defined splitting criterion based on Jacobi constant values [12]. By definition, the value of the Jacobi constant along a given trajectory remains constant. Differences in Jacobi constant between two solutions thus reflect different orbits/trajectories, whereas neighboring solutions of the same Jacobi constant likely belong to the same trajectory but separated by phase. Thus, the Jacobi constant variance serves as a strong predictor of linearization error [12]. This relationship between linearization error and Jacobi constant variance is demonstrated in Fig. 4, where the initial regression point ensemble covariance grows significantly over time. If, prior to propagation, the variance of the Jacobi constant values of the sigma-points exceeds a user-defined threshold, the component is split. It is important to note that this splitting criterion was introduced for a non-maneuvering CSO where representing a wide range of trajectories was detrimental to the performance of the filter. In this paper, with a maneuvering CSO, an unknown number of trajectories can be present thus the representation of multiple trajectories is required in the prior and posterior pdfs. However, only a single trajectory should be represented on the component level allowing for the adoption of this splitting criterion.

The Jacobi constant variance associated with the component $(\omega, \mathbf{m}, \mathbf{P})$ is given by

$$\sigma_C^2 = \int \left(C(\mathbf{x}) - \mathrm{E}\left[C(\mathbf{x})\right]\right)^2 \mathcal{N}(\mathbf{x}; \mathbf{m}, \mathbf{P}) \mathrm{d}\mathbf{x} \tag{66}$$

which can be trivially computed using the already computed regression points. The associated split criterion function is then defined as

$$c_{\mathrm{JC}}(\omega, \mathbf{m}, \mathbf{P}; \sigma_{C,\max}^2, \omega_{\min}) = \min\left(\sigma_C^2 - \sigma_{C,\max}^2,\, \omega - \omega_{\min}\right) \tag{67}$$

such that a component is split if its GM weight is larger than the minimum allowable value $w_{\min}$ and its associated Jacobi constant variance σ_C^2 exceeds the user-specified threshold $\sigma_{C,\max}^2$.

4.3 Splitting for Negative Information

In the cislunar regime, long periods of multiple sensing opportunities are rare due to solar illumination, Earth/Moon occlusion, and Earth/Moon exclusion angles. It is important to incorporate any information gained from not detecting a target, termed negative information. Negative information is incorporated into the posterior pdf via the probability of detection function $p_{D,k}^{(o)}(\mathbf{x}_k; \mathcal{S}^{(o)})$. Note that the expansion approximation applied in (46) and (47) effectively assumes the probability of detection of a single component to be constant over its local support. Thus, significant approximation errors may arise when large components overlap the sensor FoV boundaries. Such components experience a sharp change in the probability of detection within its local support. To address this, the proposed filter adopts a geometric recursive splitting algorithm that splits components that overlap FoV bounds until some stopping criteria are reached [9, 10], as seen in Fig. 3. The details of this algorithm and its associated criterion function c are omitted for brevity but can be found in [10].

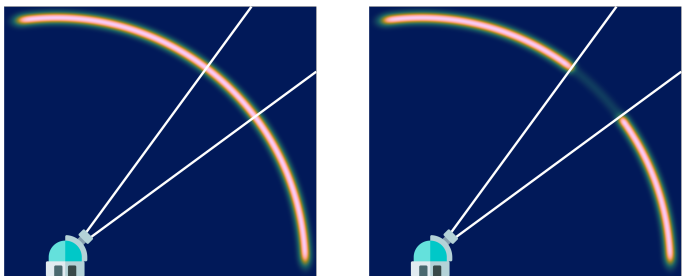

Fig. 3: Example space object state probability density function before (left) and after (right) incorporating negative information (non-detection), obtained using recursive Gaussian mixture splitting [12].

4.4 Nonlinear Constraints

The proposed filter provides the ability to add any additional nonlinear constraints or soft data from human sources. For example, with knowledge of the target's ΔV capacity, bounds can be imparted on the Jacobi constant as

$$C_{\min}(\Delta V) \leq C(\mathbf{x}) \leq C_{\max}(\Delta V) \tag{68}$$

To incorporate this constraint, components that violate the Jacobi constant bounds can be eliminated from the GM. In the context of tracking a maneuvering CSO where no knowledge of the ΔV capacity is available, a conservative minimum and maximum can be chosen that account for the maximum realistic ΔV capacity in cislunar operations. Additionally, the assumption of target-lunar collision avoidance can be incorporated into the posterior. When components are in the Moon's vicinity, they can be split in a similar manner to the application of negative information. The portion of the density within the Moon can then be truncated. These nonlinear constraints can be seen graphically in Fig. 5.

4.5 Target Modality Definitions and Discrete-Time Approximation

In a nonlinear JMS system, modes are used to differentiate between varying dynamics, measurement models, and noise covariances. To account for a maneuvering CSO, this paper assumes mode-independent dynamics, measurements, and measurement noise covariance and accounts for the potentiality of thrusting through a mode dependent process noise covariance. In particular, the proposed filter has two modes where ballistic trajectories are denoted by $\tau_k = 1$ and maneuvers are denoted by $\tau_k = 2$. The continuous-time process noise covariance for a given mode is defined as

$$\mathbf{Q}^{(j)} = \mathrm{E}[\mathbf{w}(t, \tau = j)\mathbf{w}(t, \tau = j)^\top] = \begin{bmatrix} \left(q_{w_x}^{(j)}\right)^2 & 0 & 0 \\ 0 & \left(q_{w_y}^{(j)}\right)^2 & 0 \\ 0 & 0 & \left(q_{w_z}^{(j)}\right)^2 \end{bmatrix} \tag{69}$$

The discrete-time process noise covariance mapped to the state space is found via the solution of

$$\mathbf{Q}_{k-1}^{(j)} = \int_{t_{k-1}}^{t_k} \mathbf{\Phi}(t_k, t')\mathbf{\Gamma}\mathbf{Q}^{(j)}\mathbf{\Gamma}^T\mathbf{\Phi}^T(t_k, t')dt' \tag{70}$$

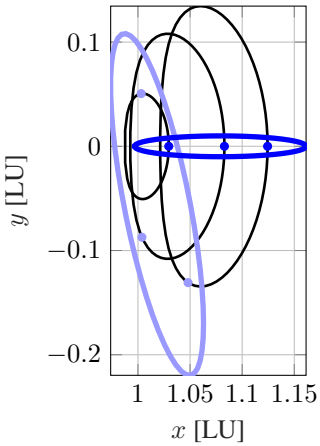

Fig. 4: Growth in covariance as a result of different Jacobi constant values where black denotes periodic halo orbits, dark blue denotes the initial points and their covariance, and light blue denotes the propagated points and their covariance.

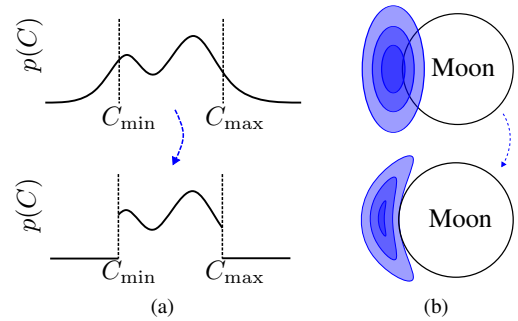

Fig. 5: Graphical depiction of the nonlinear constraints for (a) Jacobi constant bounds and (b) Moon collision.

where $\mathbf{\Phi}(t_k, t')$ is the state transition matrix from a state at $t' \in [t_{k-1}, t_k]$ to a state at t_k and

$$\mathbf{\Gamma} = \begin{bmatrix} \mathbf{0}_{3\times3} \\ \mathbf{I}_{3\times3} \end{bmatrix} \tag{71}$$

The integral in (70) does not have a closed form solution under the time varying dynamics of the CR3BP, so it is approximated through Van Loan's matrix fraction decomposition as described in [40,41]. Let $\mathbf{F}(\mathbf{x}(t'))$ be the Jacobian of the continuous-time dynamics at time t' defined as

$$\mathbf{F} = \begin{bmatrix} 0 & 0 & 0 & 1 & 0 & 0 \\ 0 & 0 & 0 & 0 & 1 & 0 \\ 0 & 0 & 0 & 0 & 0 & 1 \\ \left.\frac{\partial^2 U}{\partial x^2}\right|_{\mathbf{x}(t')} & \left.\frac{\partial^2 U}{\partial x \partial y}\right|_{\mathbf{x}(t')} & \left.\frac{\partial^2 U}{\partial x \partial z}\right|_{\mathbf{x}(t')} & 0 & 2 & 0 \\ \left.\frac{\partial^2 U}{\partial y \partial x}\right|_{\mathbf{x}(t')} & \left.\frac{\partial^2 U}{\partial y^2}\right|_{\mathbf{x}(t')} & \left.\frac{\partial^2 U}{\partial y \partial z}\right|_{\mathbf{x}(t')} & -2 & 0 & 0 \\ \left.\frac{\partial^2 U}{\partial z \partial x}\right|_{\mathbf{x}(t')} & \left.\frac{\partial^2 U}{\partial z \partial y}\right|_{\mathbf{x}(t')} & \left.\frac{\partial^2 U}{\partial z^2}\right|_{\mathbf{x}(t')} & 0 & 0 & 0 \end{bmatrix} \tag{72}$$

and assume that $\mathbf{F}(\mathbf{x}(t')) \approx \mathbf{F}(\mathbf{x}(t_{k-1}))$ for any $t' \in [t_{k-1}, t_k]$. Defining the matrix exponential

$$\exp\left(\begin{bmatrix} -\mathbf{F}(\mathbf{x}(t_{k-1}))^\top & \mathbf{\Gamma}\mathbf{Q}^{(j)}\mathbf{\Gamma}^T \\ \mathbf{0}_{6\times6} & \mathbf{F}(\mathbf{x}(t_{k-1})) \end{bmatrix}\right) = \begin{bmatrix} \mathbf{M}_{1,k-1}^{(j)} & \mathbf{M}_{2,k-1}^{(j)} \\ \mathbf{0}_{6\times6} & \mathbf{M}_{3,k-1}^{(j)} \end{bmatrix} \tag{73}$$

the discrete-time process noise mapped to the state space is approximated as

$$\mathbf{Q}_{k-1}^{(j)} \approx \left(\mathbf{M}_{3,k-1}^{(j)}\right)^\top \mathbf{M}_{2,k-1}^{(j)} \tag{74}$$

5. RESULTS

The proposed filter is tested against a simplified cislunar trajectory inspired by the Artemis I mission. Unlike the Artemis I trajectory, which has a total of 19 reported maneuvers [42], the simplified trajectory features four impulsive maneuvers designed to mimic the Artemis I outbound powered flyby (OPF), distant retrograde insertion (DRI), distant retrograde departure (DRD), and return powered flyby (RPF) maneuvers and is presented in Fig. 6. The initial epoch of the simulation is November 16, 2022, 08:44:51.150 UTC chosen to align with the timeline of the Artemis I mission, and the total simulation time is 28.30 days. The $\Delta\mathbf{v}$ magnitudes of the simplified OPF, DRI, DRD, and RPF maneuvers are 0.1980, 0.0997, 0.0997, and 0.1980 km/s, respectively. Exact details of the time and magnitudes of the maneuvers are presented in Table 1, and the initial state of the target is defined as

$$\mathbf{r}_0 = \begin{bmatrix} 75,926.589 & 56,944.942 & 0 \end{bmatrix}^\top \text{ [km]} \tag{75}$$

$$\mathbf{v}_0 = \begin{bmatrix} 1.5636 & 1.8042 & 0 \end{bmatrix}^\top \text{ [km/s]} \tag{76}$$

with an initial position and velocity uncertainty of 20 km and 1 m/s root sum square (RSS), respectively.

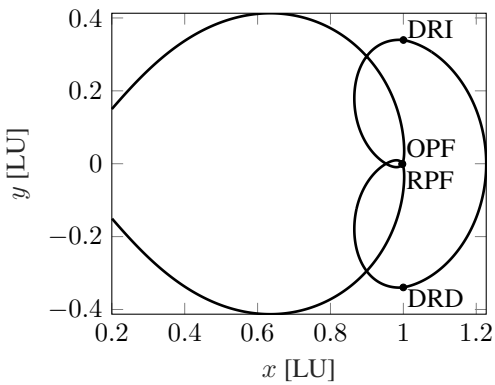

Fig. 6: Simplified Artemis I trajectory.

Table 1: Impulsive Maneuvers

Maneuver	$t - t_0$ [days]	$\Delta\mathbf{v}^\top$ [km/s]
OPF	4.6488	$\begin{bmatrix} -0.1385 & -0.1415 & 0 \end{bmatrix}$
DRI	10.1894	$\begin{bmatrix} -0.0878 & 0.0472 & 0 \end{bmatrix}$
DRD	18.1152	$\begin{bmatrix} -0.0878 & -0.0472 & 0 \end{bmatrix}$
RPF	23.6558	$\begin{bmatrix} -0.1385 & 0.1415 & 0 \end{bmatrix}$

A notional cislunar space-based surveillance network is considered that consists of three observer spacecraft in an Earth-Moon 1:1 planar resonant periodic orbit, as shown in Fig. 7, with initial conditions

$$\mathbf{r}^{(1)}_{0,\text{obs}} = \begin{bmatrix} 212,171.440 & 224,189.013 & 0 \end{bmatrix}^\top \text{ [km]}, \qquad \mathbf{v}^{(1)}_{0,\text{obs}} = \begin{bmatrix} 0.1618 & 0.5780 & 0 \end{bmatrix}^\top \text{ [km/s]} \tag{77}$$

$$\mathbf{r}^{(2)}_{0,\text{obs}} = \begin{bmatrix} 267,266.589 & 291,378.691 & 0 \end{bmatrix}^\top \text{ [km]}, \qquad \mathbf{v}^{(2)}_{0,\text{obs}} = \begin{bmatrix} 0.4596 & 0.1991 & 0 \end{bmatrix}^\top \text{ [km/s]} \tag{78}$$

$$\mathbf{r}^{(3)}_{0,\text{obs}} = \begin{bmatrix} 361,478.978 & 291,915.604 & 0 \end{bmatrix}^\top \text{ [km]}, \qquad \mathbf{v}^{(3)}_{0,\text{obs}} = \begin{bmatrix} 0.5970 & -0.1946 & 0 \end{bmatrix}^\top \text{ [km/s]} \tag{79}$$

A 1:1 resonant orbit is selected to mimic the nearly 1:1 behavior of the Sun in the synodic frame. As such, it is likely that a sensor with suitable lighting conditions at one epoch will have suitable lighting conditions at a later epoch. When visibility conditions are satisfied, angle measurements are simulated according to (9) and corrupted by white Gaussian noise with a standard deviation of 18 arcsec, which reflects a single pixel error of a camera with a $10^\circ \times 10^\circ$ FoV and 2048×2048 pixel focal plane array. For ease of analysis, the sensor attitudes are designed to track the object. Lighting conditions are simulated based on historical solar ephemerides from the Artermis I mission period, and when available, measurements are taken every 120 seconds. Fig. 7 presents the number of sensors that can measure the target along its trajectory including illumination conditions and the impact of Earth/Moon occlusion, umbra, and exclusion angles. The most impactful constraint is the Moon exclusion angle that results in long observation gaps during which the OPF and RPF maneuvers take place. The two observations gaps last for 1.686 and 2.606 days, respectively. Other pertinent parameters of the AGMIMM are presented in Table 2.

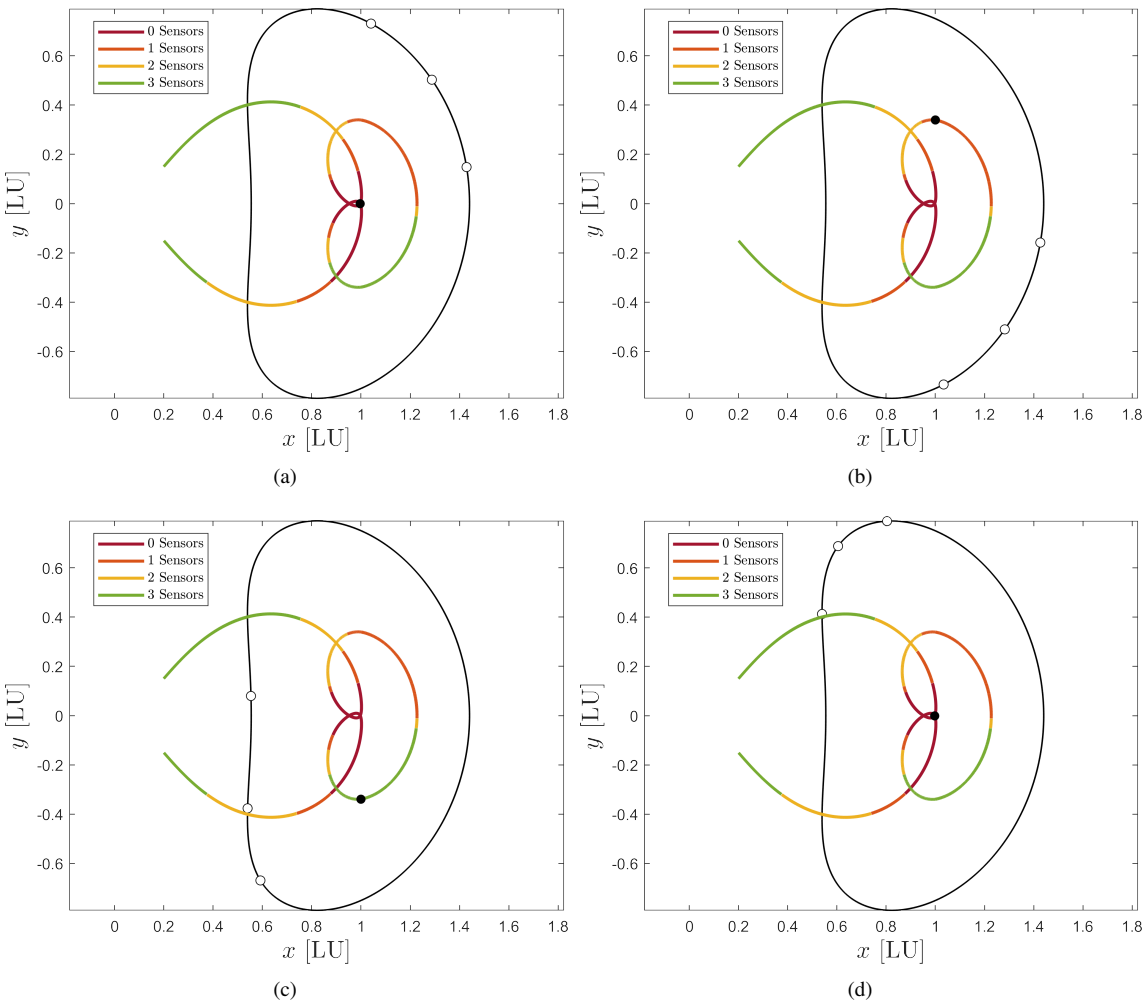

Fig. 7: Visibility of the target along the entire trajectory where colored lines denote the number of sensors that can measure the target at a given location, the black line denotes the sensors' orbit, the black dot denotes the location of the target, and black circles denote the locations of the sensors. The target and sensor geometry is show for the (a) OPF, (b) DRI, (c), DRD, and (d) RPF maneuvers.

Table 2: AGMIMM Filter Parameters

	Parameter	Value
Jump Markov Parameters	π_{11}	0.99
	π_{12}	0.01
	π_{21}	0.1
	π_{22}	0.9
Gaussian Splitting	L	50
	$s_{\max}$	0.1
	$\omega_{\min}$	0.01
	$\sigma^2_{C,\max}$	0.0001
	$C_{\min}$	$2\,[\mathrm{LU}^2/\mathrm{TU}^2]$
	$C_{\max}$	$3.5\,[\mathrm{LU}^2/\mathrm{TU}^2]$
	$q^{(1)}_{w_x}, q^{(1)}_{w_y}, q^{(1)}_{w_z}$	$0\,[\mathrm{LU}^2/\mathrm{TU}^3]$
	$q^{(2)}_{w_x}, q^{(2)}_{w_y}, q^{(2)}_{w_z}$	$1\,[\mathrm{LU}^2/\mathrm{TU}^3]$

The performance of the proposed filter is compared to that of the square-root unscented Kalman filter (SRUKF) [43], IMM [23], and GMIMM [24] in 250 Monte Carlo trials. The position and velocity estimation performance of the four filters are presented in Fig. 9. When visibility conditions permit, high-frequency multi-sensor measurements lead to nearly Gaussian distributions and the SRUKF, IMM, and GMIMM offer comparable state estimation accuracy compared to the AGMIMM. Throughout the first observation gap, however, the error and associated uncertainty of the IMM and GMIMM approach values on the order of 10^{10} km and 10^{7} m/s. The large uncertainty is also evidenced by the marginals presented in Figs. 8(b) and 8(c). The SRUKF, on the other hand, results in an error and uncertainty on the same order of magnitude as the Earth-Moon semi-major axis. The AGMIMM results in position errors one order of magnitude fewer than the semi-major axis. Figs. 8(a) and 8(d) further clarify that the resultant SRUKF uncertainty spans the cislunar regime whereas the uncertainty of the AGMIMM estimation remains in the vicinity of the Moon. Following the first observation gap, the effective range information provided by coincident observations by two observers stresses the non-adaptive filters, resulting in failure of all 250 trials of the SRUKF and IMM and 248 trials of the GMIMM. The remaining two trials of the GMIMM and the 250 trials of the AGMIMM successfully retain track custody of the target during the DRI and DRD maneuvers where at least one observer is providing measurements. At the close of the second observation gap, the remaining two trials of the GMIMM and three trials of the AGMIMM fail. A total of 247 trials of the AGMIMM successfully retained track custody through the end of the trajectory, and the cause of the three failures was a result of numerical failure in the solution of the CR3BP and not a direct limitation of the filter.

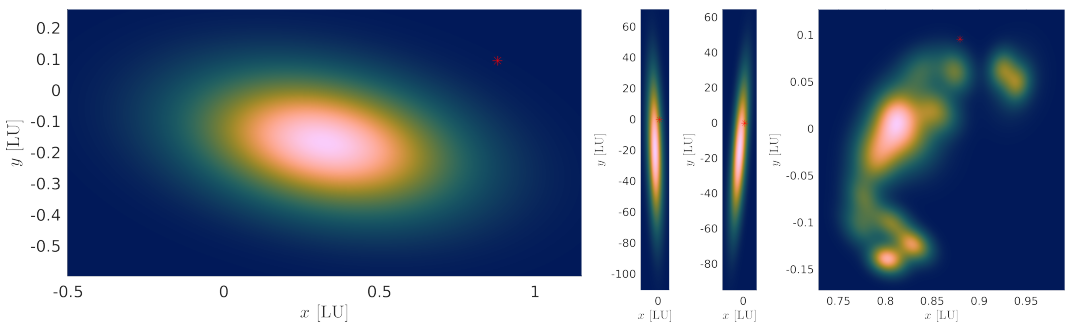

Fig. 8: Posterior state distributions marginals of the (a) SRUKF, (b) IMM, (c) GMIMM, and (d) AGMIMM at day 5.8 where the red star denotes the target truth.

6. CONCLUSION

This paper proposes a novel adaptive Gaussian mixture (AGM) filter that is uniquely able to track a maneuvering, noncooperative target in highly nonlinear, chaotic systems. The proposed adaptive Gaussian mixture interacting multiple model (AGMIMM) filter is suitable for nonlinear jump Markov systems (JMSs) where the target modality evolves according to a homogeneous Markov chain. Cluster-based merging is employed to maintain computational tractability while retaining accurate descriptions of the non-Gaussian state uncertainty. Furthermore, the AGMIMM employs multi-criterion parametric adaptation to account for nonlinear effects due to dynamics, measurements, negative information, and known constraints. The AGMIMM is analyzed in a 250-trial Monte Carlo cislunar object tracking simulation and shown to significantly outperform existing maneuvering target tracking algorithms in terms of state estimation accuracy and robustness. Further work in the topic of maneuvering target tracking in nonlinear/chaotic systems will consider multi-object systems and clutter.

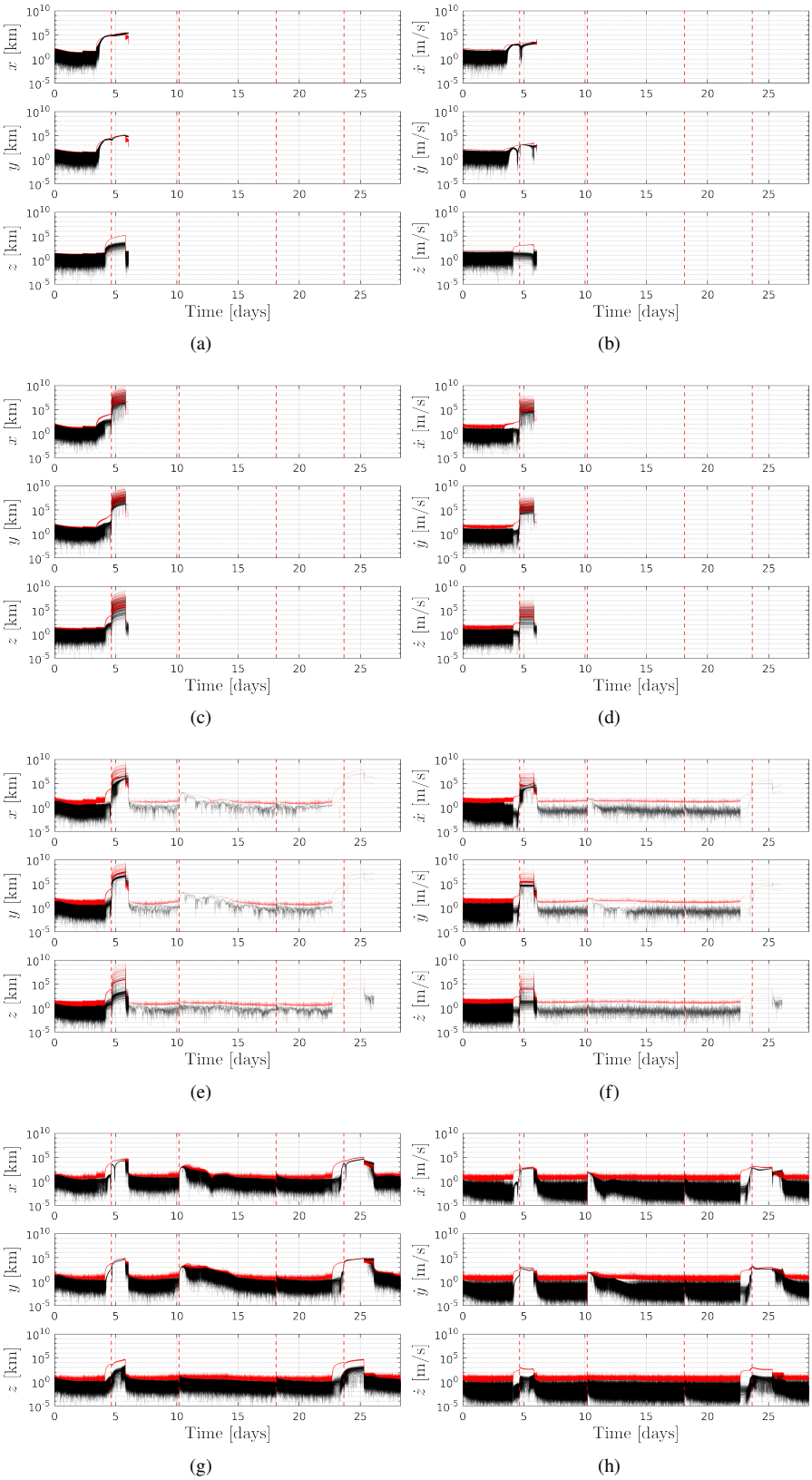

Fig. 9: Position (a,c,e,g) and velocity (b,d,f,h) estimation performance over 250 Monte Carlo trials of the SRUKF (a,b), IMM (c,d), GMIMM (e,f), and AGMIMM (g,h) where black denotes the estimation error, red denotes the uncertainty in terms of the error variance 3σ bounds, and red dashed lines mark the maneuvers.

REFERENCES

[1] Nagavenkat Adurthi and Puneet Singla. Conjugate Unscented Transformation-Based Approach for Accurate Conjunction Analysis. *Journal of Guidance, Control, and Dynamics*, 38(9):1642–1658, September 2015.

[2] Keith A. LeGrand, Pingping Zhu, and Silvia Ferrari. Cell Multi-Bernoulli (Cell-MB) Sensor Control for Multi-Object Search-While-Tracking (SWT). *IEEE Transactions on Pattern Analysis and Machine Intelligence*, 45(6):7195–7207, June 2023.

[3] Augustus Buonviri, Matthew York, Keith Allen LeGrand, and James Meub. Survey of Challenges in Labeled Random Finite Set Based Distributed Multi-sensor Multi-object Tracking. In *2019 IEEE Aerospace Conference*, 2019.

[4] Maaninee Gupta, Kathleen C Howell, and Carolin Frueh. Constellation design to support cislunar surveillance leveraging sidereal resonant orbits. In *33rd AAS/AIAA Space Flight Mechanics Meeting*, 2023.

[5] Uwe D Hanebeck, Kai Briechle, and Andreas Rauh. Progressive Bayes: a new framework for nonlinear state estimation. In *Multisensor, Multisource Information Fusion: Architectures, Algorithms, and Applications 2003*, volume 5099, pages 256–267. SPIE, 2003.

[6] Marco F Huber, Tim Bailey, Hugh Durrant-Whyte, and Uwe D Hanebeck. On entropy approximation for Gaussian mixture random vectors. In *2008 IEEE International Conference on Multisensor Fusion and Integration for Intelligent Systems*, pages 181–188. IEEE, 2008.

[7] Kyle J DeMars, Robert H Bishop, and Moriba K Jah. Entropy-based approach for uncertainty propagation of nonlinear dynamical systems. *Journal of Guidance, Control, and Dynamics*, 36(4):1047–1057, 2013.

[8] Kirsten Tuggle and Renato Zanetti. Automated Splitting Gaussian Mixture Nonlinear Measurement Update. *Journal of Guidance, Control, and Dynamics*, 41(3), 2018.

[9] K. LeGrand and S. Ferrari. The role of bounded fields-of-view and negative information in finite set statistics (FISST). In *Proceedings of 2020 23rd International Conference on Information Fusion, FUSION 2020*, 2020.

[10] Keith A. LeGrand and Silvia Ferrari. Split Happens! Imprecise and Negative Information in Gaussian Mixture Random Finite Set Filtering. *Journal of Advances in Information Fusion*, 17(2):78–96, December 2022.

[11] Kumar Vishwajeet and Puneet Singla. Adaptive Split/Merge-Based Gaussian Mixture Model Approach for Uncertainty Propagation. *Journal of Guidance, Control, and Dynamics*, 41(3):1–15, 2017.

[12] Keith A LeGrand, Aneesh V Khilnani, and John L Iannamorelli. Bayesian angles-only cislunar space object tracking. In *33rd AAS/AIAA Space Flight Mechanics Meeting*, 2023.

[13] Reza Madankan, Puneet Singla, Tarunraj Singh, and Peter D. Scott. Polynomial-Chaos-Based Bayesian Approach for State and Parameter Estimations. *Journal of Guidance, Control, and Dynamics*, 36(4):1058–1074, July 2013.

[14] Brandon A Jones, Alireza Doostan, and George H Born. Nonlinear Propagation of Orbit Uncertainty Using Non-Intrusive Polynomial Chaos. *Journal of Guidance, Control & Dynamics*, 36(2):430, March 2013.

[15] Brandon A Jones. Multi-Fidelity Methods for Orbit Determination. In *Proceedings of the Advanced Maui Optical and Space Surveillance Technologies Conference (AMOS)*, 2018.

[16] Ashwin Carvalho, Yiqi Gao, Stéphanie Lefevre, and Francesco Borrelli. Stochastic predictive control of autonomous vehicles in uncertain environments. In *12th International Symposium on Advanced vehicle control*, volume 9, 2014.

[17] Zhongzhen Luo, Mina Attari, Saeid Habibi, and Martin Von Mohrenschildt. Online multiple maneuvering vehicle tracking system based on multi-model smooth variable structure filter. *IEEE Transactions on Intelligent Transportation Systems*, 21(2):603–616, 2019.

[18] Robert H Bishop and AC Antoulas. Nonlinear approach to aircraft tracking problem. *Journal of Guidance, Control, and Dynamics*, 17(5):1124–1130, 1994.

[19] Haowei Zhang, Junwei Xie, Jiaang Ge, Wenlong Lu, and Binfeng Zong. Adaptive strong tracking square-root cubature Kalman filter for maneuvering aircraft tracking. *IEEE Access*, 6:10052–10061, 2018.

[20] Ying Chen, Zhen Cheng, and Shuliang Wen. Nonlinear filters for tracking maneuverable ballistic missile targets on reentry. 2009.

[21] Antonio San Jose. Theater ballistic missile defense–multisensor fusion, targeting and tracking techniques. *Master of Science in Electrical Engineering from the Naval Postgraduate School*, pages 5–7, 1998.

[22] Yaakov Bar-Shalom, X Rong Li, and Thiagalingam Kirubarajan. *Estimation With Applications to Tracking and Navigation: Theory Algorithms and Software*. John Wiley & Sons, 2001.

[23] Henk AP Blom and Yaakov Bar-Shalom. The interacting multiple model algorithm for systems with Markovian

switching coefficients. *IEEE Transactions on Automatic Control*, 33(8):780–783, 1988.

[24] Dann Laneuville and Yaakov Bar-Shalom. Maneuvering target tracking: A Gaussian mixture based IMM estimator. In *2012 IEEE Aerospace Conference*, pages 1–12. IEEE, 2012.

[25] Li Wang, Yan Liang, Xiaoxu Wang, and Linfeng Xu. Gaussian sum filter of Markov jump non-linear systems. *IET Signal Processing*, 9(4):335–340, 2015.

[26] Hans Driessen and Yvo Boers. An efficient particle filter for jump Markov nonlinear systems. In *IEE Target Tracking 2004: Algorithms and Applications*, pages 19–22. IET, 2004.

[27] André R Braga, Carsten Fritsche, Fredrik Gustafsson, and Marcelo GS Bruno. Rapid system identification for jump Markov non-linear systems. In *2017 IEEE 7th International Workshop on Computational Advances in Multi-Sensor Adaptive Processing (CAMSAP)*, pages 1–5. IEEE, 2017.

[28] Syed Ahmed Pasha, Ba-Ngu Vo, Hoang Duong Tuan, and Wing-Kin Ma. A Gaussian mixture PHD filter for jump Markov system models. *IEEE Transactions on Aerospace and Electronic systems*, 45(3):919–936, 2009.

[29] Marcus J. Holzinger, Daniel J. Scheeres, and Kyle T. Alfriend. Object Correlation, Maneuver Detection, and Characterization Using Control Distance Metrics. *Journal of Guidance, Control, and Dynamics*, 35(4):1312–1325, July 2012.

[30] J Greaves and D Scheeres. Optical only co-estimation and maneuver classification in the cislunar regime. In *Rocky Mountain AAS GNC Conference*, pages 22–041, 2022.

[31] Jesse Greaves and Daniel Scheeres. Maneuver detection for cislunar vehicles using optical measurements. In *Advanced Maui Optical and Space Surveillance Technologies Conference (AMOS)*, 2020.

[32] Karina Rivera, Anthony Zara, Daniel Aguilar-Marsillach, Marcus Holzinger, Ian Elliott, and Natasha Bosanac. Patterns of life and maneuver detection for cislunar trajectory maintenance. In *22nd Advanced Maui Optical and Space Surveillance Technologies Conference (AMOS), Maui, HI*, 2021.

[33] Jesse A Greaves and Daniel J Scheeres. Relative estimation in the cis-lunar regime using optical sensors. In *Proceedings of the Advanced Maui Optical and Space Surveillance Technologies Conference*, 2021.

[34] Ba Tuong Vo, Chong Meng See, Ning Ma, and Wee Teck Ng. Multi-sensor joint detection and tracking with the Bernoulli filter. *IEEE Transactions on Aerospace and Electronic Systems*, 48(2):1385–1402, 2012.

[35] Charles J Wetterer, C Channing Chow II, Baldwin Jason, Micah Dilley, Keric Hill, Helen Montell-Weiland, Paul Billings, Christopher Craft, and James Frith. Cislunar maneuver detection and classification. In *Advanced Maui Optical and Space Surveillance Technologies Conference (AMOS)*, 2022.

[36] Dennis Schieferdecker and Marco F Huber. Gaussian mixture reduction via clustering. In *2009 12th International Conference on Information Fusion*, pages 1536–1543, 2009.

[37] Andrew R Runnalls. Kullback-Leibler approach to Gaussian mixture reduction. *IEEE Transactions on Aerospace and Electronic Systems*, 43(3):989–999, 2007.

[38] Harold W Sorenson and Daniel L Alspach. Recursive Bayesian estimation using Gaussian sums. *Automatica*, 7(4):465–479, 1971.

[39] Marco F Huber. Adaptive Gaussian mixture filter based on statistical linearization. In *14th International Conference on Information Fusion*, pages 1–8. IEEE, 2011.

[40] Patrik Axelsson and Fredrik Gustafsson. Discrete-time solutions to the continuous-time differential Lyapunov equation with applications to Kalman filtering. *IEEE Transactions on Automatic Control*, 60(3):632–643, 2014.

[41] Charles Van Loan. Computing integrals involving the matrix exponential. *IEEE Transactions on Automatic Control*, 23(3):395–404, 1978.

[42] Jacob Sullivan and Christopher D'Souza. Extended Kalman filter performance on the Artemis-1 mission. In *45th Rocky Mountain AAS GN&C Conference*, number AAS 23-053, 2023.

[43] Rudolph Van Der Merwe. *Sigma-point Kalman Filters for Probabilistic Inference in Dynamic State-space Models*. Oregon Health & Science University, 2004.